Vanselow, Christoph ; Stöbener, Dirk ; Kiefer, Johannes ; Fischer, Andreas

Particle image velocimetry in refractive index fields of combustion flows

Particle image velocimetry in refractive index fields of combustion flows

Christoph Vanselow[1] [iD] · **Dirk Stöbener[1,3]** · **Johannes Kiefer[2,3]** · **Andreas Fischer[1,3]**

Abstract

Optical measurements inside reacting flows are often disturbed by refractive index fields, e.g., due to the strong density gradients in flames. Although occurring measurement errors due to light refraction are a known problem for certain particle image velocimetry (PIV) applications, only a qualitative analysis of the resulting measurement uncertainty inside flame flows has been carried out to date. As an important step forward, a measurement approach is proposed, which enables a quantification of the resulting measurement uncertainties due to light refraction. As an example, the measurement approach is applied to a premixed propane flame. The uncertainty analysis is based on the determination of occurring particle position errors due to light refraction inside the flame. For three different measurement planes, the velocity field is measured with PIV and the particle position errors are experimentally measured and verified by ray-tracing simulation based on the measured refractive index field, which is determined by the background-oriented Schlieren method. In the examined flow, maximal position errors amount up to 14 μm and yield significant systematic velocity errors of up to 4% and random velocity errors of up to 6%. In contrast to the systematic velocity error, the random velocity error varies significantly for the analyzed measurement planes inside the flame flow.

Graphic abstract
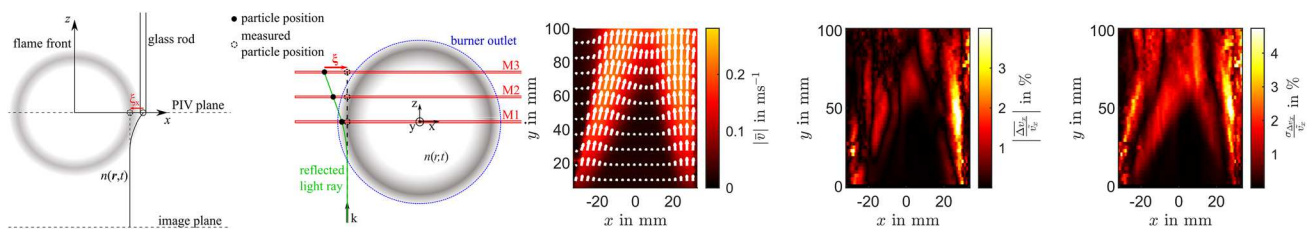
1 Introduction

Particle image velocimetry (PIV) provides optical measurements of flow velocity fields, which are essential for combustion diagnostics (Fischer et al. 2013; Steinberg et al. 2010; Fischer 2017). The measurement principle is to seed small particles (typical diameter ≈ 1 μm) into the flow, which follow the flow with negligible slip. The particle laden flow is illuminated by a laser light sheet and two timely separated particle images are taken. The flow velocity field is approximated by the particle movement determined by cross-correlation-based evaluation of the timely separated images. The typical PIV measurement uncertainty is about 1–2% (Westerweel 1997; Voges et al. 2007) and is caused, for example, by photon shot noise (Fischer 2016) and other intensity variations of the particle images (Nobach and Bodenschatz 2009). Especially for PIV measurements inside combustion flows, the measurement is further disturbed by light emissions of the flames and inhomogeneous refractive index fields.

✉ Christoph Vanselow
  c.vanselow@bimaq.de

[1] Bremen Institute for Metrology, Automation and Quality Science (BIMAQ), University of Bremen, Linzer Str. 13, 28359 Bremen, Germany

[2] Technische Thermodynamik, University of Bremen, Badgasteiner Str. 1, 28359 Bremen, Germany

[3] MAPEX Center for Materials and Processes, University of Bremen, Bibliothekstrae 1, 28334 Bremen, Germany

1

The latter cause light ray deflections in the illumination path and the observation light path from the particle to the camera. While light emissions of the flame can easily be filtered out by bandpass filters with a center wavelength of the PIV laser light illumination (typically 532 nm) (Raffel et al. 2002), the influence of the light deflection inside the inhomogeneous refractive index field leads to inevitable particle image distortions and image blurring (Elsinga et al. 2005). A measurement error of the particle positions and a reduction of the signal-to-noise ratio are the consequences.

The amount of the light refraction depends on the gradient of the refractive index field and the distance of the light path inside the inhomogeneous refractive index field. The refractive index field depends on the density distribution of the optical media influenced by temperature and pressure fields. In addition, for measurements in reacting or multiple phase media (e.g., flames, aerosols, and sprays), the refractive index field also depends on the distribution and condition of the individual species. Since the resulting refractive index field depends on various parameters, investigations of the resulting PIV measurement uncertainty is generally performed by the measurement of the resulting light refraction itself throughout the refractive index field for an estimation of the amount of light refraction in the measurement plane, which is usually located inside the refractive index field.

The background-oriented Schlieren (BOS) technique measures the light refraction throughout the refractive index field by observing a synthetic pattern placed in the background of the refractive index field. Image distortions of the observed pattern result from light refraction integrated throughout the refractive index field. Thus, a symmetry assumption is necessary for a spatial reconstruction of the refractive index field (Tan et al. 2015). BOS measurements in supersonic flows were performed by Elsinga et al. to correct PIV measurement errors of about 2–3% caused by pressure fields with the assumption of a constant gradient of the refractive index in the line-of-sight direction of the camera (Elsinga et al. 2005). Since a symmetry condition is necessary, the standard BOS technique is not applicable for refractive index fields with asymmetric fluctuations induced by, e.g., turbulence.

The resulting measurement uncertainties inside flame flows due to refractive index fields were qualitatively analyzed in Stella et al. (2001). The deflection of the light rays propagating through a premixed flame was measured. The light refraction mainly takes place in the flame front, where the highest temperature and hence refractive index gradients are located. Light sheet deflection leads to a curved measurement plane, but in combustion flows at laboratory scale, the resulting PIV measurement uncertainty can be neglected. The refractive index field causes image distortion. The result

is a decrease of the signal-to-noise ratio and particle position errors. In addition, the measurement error caused by varying position errors between the successive particle images is negligible if the time interval between the laser pulses is small compared to the characteristic timescales of the flame front deformation. However, no quantitative information about the resulting measurement errors was given. Furthermore, the movement of the particles in a curved refractive index field was not considered.

In contrast to the measurement of the resulting light refraction, the refractive index field of a hot jet was recently determined by means of the measured temperature field for an estimation of the resulting PIV measurement uncertainty (Vanselow and Fischer 2018). For triangulated particle positions, as it is performed in the calibration procedure in stereoscopic PIV and in tomographic PIV, the resulting particle position error was proven to be generally larger than for standard PIV measurements. The velocity error in the mean flow of the examined hot jet flow with a maximal temperature of 191 °C does not result in a significant measurement uncertainty. However, ray-tracing simulation for temperature fields with a maximum temperature of one order of magnitude larger than those occurring inside combustion flows show significant systematic measurement errors.

Another method for the estimation of the resulting PIV measurement errors caused by fluctuating refractive index fields was performed by the comparison between PIV measurement results with a reference measurement (Schlüßler et al. 2014). The influence of the fluctuating light refraction was examined for an experimental setup, where the scattering path from the particles to the camera was disturbed by a turbulent propane gas flame and a glass plate contaminated with oil droplets. The resulting velocity error depends on the velocity gradient of the examined flow. Image blurring due to light refraction results in an increased systematic measurement uncertainty of up to 10%. However, the measurement object was a jet flow, which was measured through the refractive index fields. Thus, the determined measurement uncertainty cannot be transferred to flow measurements inside combustion systems.

In the existing literature, only qualitative uncertainty estimations were performed for PIV measurements inside combustion flows. Mostly, indirect measurements of the resulting light refraction due to refractive index fields were performed to estimate the resulting PIV measurement uncertainty. The present article proposes an experimental method for a direct measurement of the resulting light refraction inside flame flows. The direct measurement approach measures the resulting particle position errors inside the PIV measurement plane. The known position of a glass rod tip located in the measurement plane is measured and the difference between the known position and the measured position is approximately the PIV particle position error. The determined

position error allows a quantification of the resulting measurement uncertainty caused by the refractive index field. The direct measurement approach is compared to the indirect background-oriented Schlieren technique. The principles of both methods are described in Sect. 2. The setups for the performed direct and indirect measurements of light refraction as well as PIV measurements inside a premixed flame are depicted in Sect. 3. The comparison between the direct and the indirect measurements of the resulting particle position errors inside the examined flame and the results of the performed PIV measurements are presented in Sect. 4. Additionally, the resulting systematic and random PIV measurement errors are quantified. Finally, the conclusions and an outlook are given in Sect. 5.

2 Measurement principle

The PIV measurement error inside a combustion flow due to light refraction is estimated by means of the resulting particle position error. The principle of the direct particle position error measurement and the indirect background-oriented Schlieren technique are described in Sect. 2.1 and in Sect. 2.2, respectively, and the determined position errors allow a calculation of resulting velocity errors.

2.1 Direct measurement of the particle position error

PIV measurements inside combustion flows are disturbed by a generally time-dependent inhomogeneous refractive index field $n(\mathbf{r}, \mathbf{t})$ with $\mathbf{r} = (x, y, z)^\mathrm{T}$, which causes image blurring and measurement errors of the particle positions. The light deflection of the scattered light on its path from a particle to the camera results in a detection of a particle actually positioned at $\mathbf{r}_\mathrm{P} = (x_\mathrm{P}, y_\mathrm{P}, z_\mathrm{P})^\mathrm{T}$ at a false position $\mathbf{r}_\mathrm{P'} = (x_\mathrm{P'}, y_\mathrm{P'}, z_\mathrm{P'})^\mathrm{T}$ in the light sheet plane at (x, y, z_P). In premixed flames, the resulting particle position error $\boldsymbol{\xi} = \mathbf{r}_\mathrm{P'} - \mathbf{r}_\mathrm{P}$ is mainly caused by temperature gradients located in the region of the flame front (Stella et al. 2001). A theoretical description of the particle position error and the resulting PIV measurement error depending on the refractive index field can be found in Vanselow and Fischer (2018) for standard, stereoscopic and tomographic PIV. To determine the particle position error $\boldsymbol{\xi}$, a direct measurement of the light deflections is performed, whereby the known position of a glass rod tip is measured inside a flame by a camera. The difference between the measured position of the glass tip $\mathbf{r}_{G'}$ and the known position $\mathbf{r}_G$ is approximately the particle position error $\boldsymbol{\xi} = \mathbf{r}_\mathrm{P'} - \mathbf{r}_\mathrm{P} \approx \mathbf{r}_{G'} - \mathbf{r}_G$, cf. Fig. 1. It is assumed that the insertion of a glass rod into the flame does not significantly affect the refractive index field on the optical path from the glass tip to the camera. A statistical
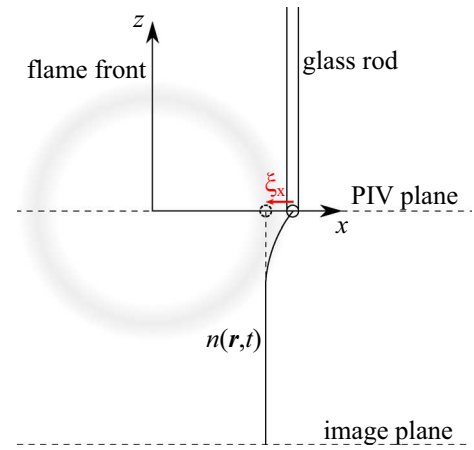

Fig. 1 Particle position error ξ_x in x-direction caused by light deflection of the scattered light from the glass rod in the PIV plane to the camera in the image plane. In premixed flames, the refractive index field is mainly caused by the temperature field located in the flame front

analysis is finally performed to determine the mean particle position error $\overline{\boldsymbol{\xi}}$ and the standard deviation of the particle position error $\sigma_{\boldsymbol{\xi}}$. The glass tip is illuminated by a pulse laser with a pulse duration of 1 ns to achieve negligible time averaging during the image acquisition. The velocity error $\Delta\mathbf{v}(\mathbf{r})$ of the performed PIV measurements is quantified by means of the position error $\boldsymbol{\xi}$ measured by the glass rod with

$$\Delta v_i = (\nabla_i \xi_i)v_i - (\nabla_i v_i)\xi_i, \tag{1}$$

which is provided by Elsinga et al. (2005). Here, $\mathbf{v} = (v_x, v_y, v_z)^\mathrm{T}$ is the measured velocity and $i = x, y, z$ denotes the component in the x, y, or z-directions. It is assumed that the fluctuations of the refractive index field are the dominant source of the standard deviation of the measured particle position error. The assumption allows an estimation of the resulting random velocity errors caused by the refractive index fluctuations using error propagation for the velocity error $\Delta\mathbf{v}$ calculated with Eq. (1):

$$\sigma_{\Delta v_i} = \sqrt{\left(\frac{\partial \Delta v_i}{\partial \xi_i}\sigma_{\xi_i}\right)^2 + \left(\frac{\partial \Delta v_i}{\partial v_i}\sigma_{v_i}\right)^2 + 2\frac{\partial}{\partial \xi_i}\frac{\partial}{\partial v_i}\mathrm{cov}(\xi_i, v_i)}$$
$$\approx \sqrt{\left(\nabla v_i \sigma_{\xi_i}\right)^2 + \left(\nabla \xi_i \sigma_{v_i}\right)^2}, \tag{2}$$

where $\sigma_{\Delta v_i}$, σ_{ξ_i}, and σ_{v_i} are the standard deviations of Δv_i, ξ_i, and v_i, respectively, and $\mathrm{cov}(\xi_i, v_i)$ is the covariance of ξ_i and v_i. A positive covariance term can be expected, due to the fact, that high velocities and large particle position errors are located in the flame front. Furthermore, the formation mechanism of increased velocity and increased light refraction arises from the heating of the fluid, which leads to expansion and convection, and a reduction of the local density varying

the refractive index. Moreover, it can be assumed that the covariance term is relative small due to the fact that the velocity field is measured inside the PIV measurement plane and the particle position error arise from the refractive index field on the optical path from the measurement plane to the camera. Therefore, a lower limit of the actual random error is estimated, resulting in a best case scenario. Thus, beside the resulting systematic PIV measurement errors, also the random errors caused by the refractive index fluctuations can be estimated by the comparatively simple measurement approach.

2.2 Indirect background-oriented Schlieren technique

As a reference method to the direct measurement of the particle position error, ray-tracing simulations based on the mean refractive index field measured by the background-oriented Schlieren technique (BOS) are performed to determine the mean particle position error $\overline{\xi}_{BOS}$. For BOS measurements, the Abel inversion allows the reconstruction of the three-dimensional refractive index field with the information of one camera perspective if the refractive index exhibits an axisymmetric distribution (Raffel 2015). However, in turbulent flames, the refractive index field is time dependent, and therefore, the instantaneous refractive index field is generally asymmetric. Hence, for axisymmetric burners, the averaged results of the light deflection measurements can only be used to determine the mean axisymmetric refractive index field of the flame. In this work, the reconstruction of the mean axisymmetric refractive index field is performed by the Abel–Fourier–Hankel method described in Tan et al. (2015), where the radial distributed refractive index field $n(r)$ with $r = \sqrt{x^2 + z^2}$ is determined for an axisymmetric refractive index distribution with the symmetry axis at $x = 0$ and $z = 0$. The index field is determined based on the measured mean deflection angles $\varepsilon = \tan^{-1}\left(\frac{\overline{\xi}_x}{d_1}\right)$ with the measured mean position error $\overline{\xi}_x$ in x-direction and the distance d_1 between the pattern in the background and the refractive index field in the camera viewing direction $\mathbf{k} = (0, 0, z)^{T}$, cf. Fig. 2. The mean position error $\overline{\xi}_x$ in x-direction is determined by the averaged results of a cross-correlation-based PIV evaluation of the distorted (flame on) and the undistorted (flame off) image of the pattern in the background recorded by the camera.

The used discrete Abel–Fourier–Hankel method calculates the mean refractive index field in the x, z-plane perpendicular to the symmetry axis by

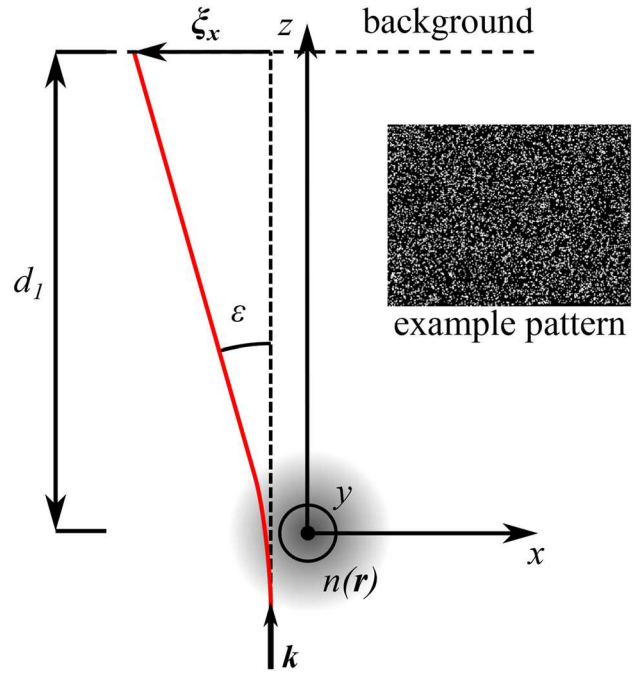$$n(r_i) = \left(\sum_{j=0}^{N} D_{ij}\varepsilon_j + 1\right) \cdot n_0, \tag{3}$$

Fig. 2 Determination of the position error ξ_x induced by the refractive index field of the axisymmetric burner by analysis of occurring image distortions of a well-known pattern placed in the background of the refractive index field

where

$$D_{ij} = -\frac{\alpha}{N}\sum_{k=0}^{[N/\alpha]} \sin\left(\frac{\alpha\pi jk}{N}\right) J_0\left(\frac{\alpha\pi ki}{N}\right) \tag{4}$$

with a smoothing coefficient α, the zero-order Bessel function J_0 and the ambient refractive index of the air at room temperature $n_0 = 1.000283$. The squared brackets $[N/\alpha]$ denotes the closest less or equal integer of the fraction. N is the number of measurement points, on which the equidistant deflection angles ε_j of the projections through the refractive index field are measured. The parameter $n(r_i)$ is the reconstructed refractive index field with identical radial equidistant spacing as the measured deflection angles. Since the deflection angles ε_j are point symmetric with respect to the x-axis due to the axisymmetry, only one half-axis of the planar measurement is necessary for a three-dimensional reconstruction.

Based on the reconstructed refractive index field, ray-tracing simulations according to Sharma et al. (1982) are performed to determine the light refraction inside the flame, which allows a simulative determination of the mean particle position error $\overline{\xi}_{BOS}$.
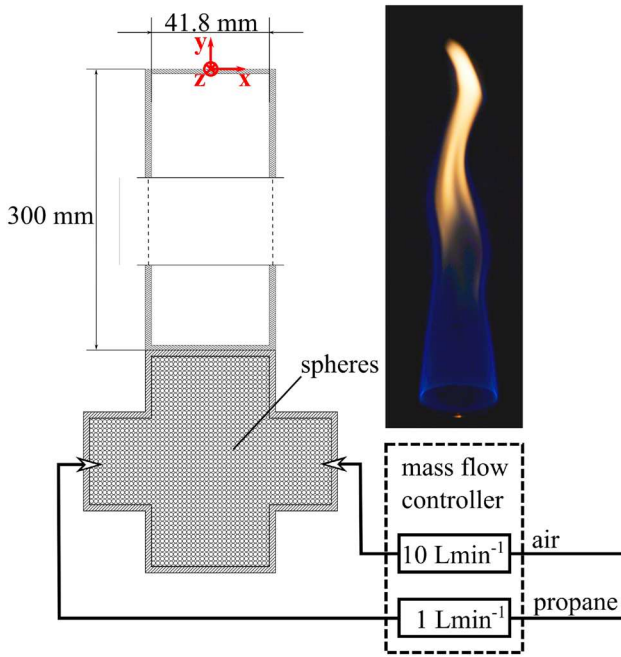
Fig. 3 Schematic of the burner with the sphere filled mixing chamber and the resulting flame for a propane inflow of $1 \, \text{L} \, \text{min}^{-1}$ and an air inflow of $10 \, \text{L} \, \text{min}^{-1}$

3 Experimental setup

In this section, the experimental setups are described. The measurement object is a premixed propane flame and its properties are described in Sect. 3.1. The setups of the direct position error measurement and the indirect BOS measurement are described in Sects. 3.2 and 3.3, respectively. The velocity field of the flame flow is measured with PIV, see Sect. 3.4.

3.1 Measurement object

The schematic of the burner with a radial symmetric outlet and the examined premixed propane flame are shown in Fig. 3. The premixing chamber of the burner is filled with spheres ($\emptyset = 5 \, \text{mm}$), which homogenize the flow to prevent unintended flow characteristics in the burner outlet. The gas composition is set by a propane ($1 \, \text{L} \, \text{min}^{-1}$) and an air ($10 \, \text{L} \, \text{min}^{-1}$) inflow resulting in an equivalence ratio of $\phi = 2.4$. The burner outlet consists of a pipe with a diameter of 41.8 mm and a length of 300 mm. It provides a laminar flow condition. The resulting flame tends to fluctuate particularly in the diffusive region of the flame, cf. Fig. 3. These fluctuations can be explained by buyoancy effects (Nogenmyr et al. 2010).

3.2 Direct light ray deflection measurement

The resulting measurement errors $\xi(\mathbf{r})$ of the particle positions inside the flame are determined by the measurement of the known position of a glass rod tip with a diameter of 1.3 mm inserted into the flame from the opposite of the camera viewing direction, cf. Fig. 4a. Compared to the typical particle size in PIV measurements of a few micrometers, the glass rod diameter is three orders of magnitude larger, which leads to an averaging effect. Thus, the measured position error inside the flame is spatially low pass filtered, which leads to an underestimation of the occurring position errors. In the PIV evaluation, also an averaging effect will result by the interrogation window size. The 1.3 mm diameter of the glass rod results in a measurement area of about $1.3 \, \text{mm}^2$. In the performed PIV evaluation, the used interrogation window size of $16 \times 16 \, \text{px}^2$ and the image size of one pixel of $56 \, \mu\text{m}$ result in a measurement area of $0.8 \, \text{mm}^2$. Thus, the
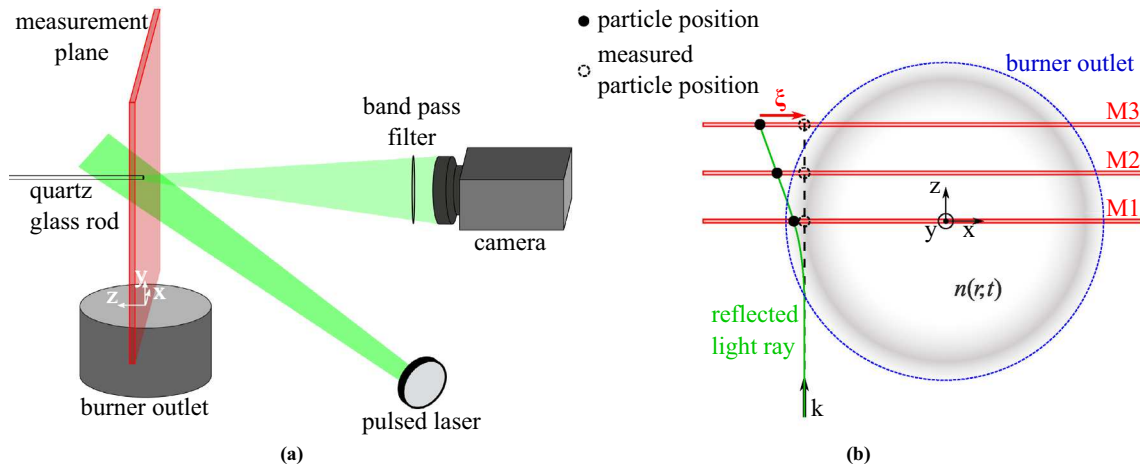

Fig. 4 Schematic of the direct measurement of the particle position error inside the flame flow. **a** Measurement setup for the position error ξ. **b** Measurement planes M1, M2, and M3 in top view of the burner outlet

averaging affect of the interrogation window is overcompensated within the measurement setup.

The position dependent error $\xi(\mathbf{r})$ of the glass tip position is determined by the relative movement of the burner with a linear positioning table. It is assumed that the refractive index field in the optical path from the glass tip to the camera is not significantly disturbed by the glass rod. Using laser illumination with the laser wavelength (532 nm), as it is used in the PIV measurements and a bandpass filter with a center wavelength of 532 nm at the camera prevent a variation of the refractive index due to the wavelength dependency. In addition, light emissions of the flame are filtered. A laser pulsewidth of 1 ns results in a negligible time averaging.

The influence of the optical path length inside the refractive index field on the resulting position error $\xi(\mathbf{r})$ is analyzed by considering three measurement planes M1, M2, and M3, cf. Fig. 4b. M1 is located perpendicular to the z-axis in the center of the burner outlet containing the symmetry axis, and M2 and M3 are located $z = 3$ mm and $z = 6$ mm in viewing direction $\mathbf{k}$ of the camera, respectively. The expected increase of the particle position error ξ with respect to the more distant measurement planes M2 and M3 will also have an effect on the PIV measurement error, which is determined in this article.

The material selection of the rod is decisive for the feasibility and accuracy of the measurement. The cross sensitivity of a possible bending of the glass rod due to flow forces is negligible. This was tested by the measurement of the glass tip position in an air flow with a higher volume flow compared to the combined propane and air flow of the flame. Furthermore, the material must withstand the high temperatures of the flame and be inert not to corrode. The manufacturer of the used quartz glass rod, Quarzglas Komponenten und Service QCS GmbH, indicates a quartz glass-softening temperature of 1730 °C, which is not reached in the examined premixed propane flame, see the temperature estimation in Sect. 4.2. Besides the high softening temperature of quartz glass, it also has a small thermal expansion constant of about 0.6×10^{-6} K compared to most metals. The influence of thermal expansion was tested by a locally heating of the rod during a measurement. Experiments with steel and wolfram were also performed indicating significant cross sensitivity of thermal expansion with steel and the forming process of wolfram oxide at the tip of the rod, respectively. Thus, quartz glass is a good choice for the rod material. However, for flames with higher temperatures than the quartz glass-softening temperature of 1730 °C and flames with much higher flow velocities than the examined propane flame, significant cross sensitivities can occur. Though, a larger diameter of the glass rod could compensate the influence of increased bending due to flow forces.

3.3 Indirect BOS measurement

A reference $\overline{\xi}_{BOS}$ to the measured systematic position error $\overline{\xi}$ is given by ray-tracing simulation based on the mean refractive index field measured with BOS. For the BOS measurement, the same camera is used as for the PIV measurement and is placed at $z = -25$ cm. In the background of the flame at $z = 60$ cm, a synthetic statistical particle pattern is positioned and observed by the camera. The particle pattern is illuminated by a high-power LED with a center wavelength of 532 nm and the particle diameter is about twice the displayed diameter of one pixel. Again, a bandpass filter with a center wavelength of 532 nm is used to filter the light emission of the flame.

3.4 PIV measurement setup

The velocity field $\mathbf{v}(\mathbf{r})$ of the flame is measured by PIV in three measurement planes M1, M2, and M3, cf. Fig. 4b. The laser light sheet illumination (thickness < 0.5 mm) is implemented by a dual-pulse laser with 200 mJ pulse energy and a pulse length of less than 10 ns (Quantel Evergreen). The flow is seeded by titanium dioxide particles with a mean diameter of 0.4 μm. For observation, a 5.5 Mpx sCMOS camera (Andor Zyla) is positioned at $z = -60$ cm viewing in the positive z-direction with a 50 mm focal length objective (Zeiss Planar T* 1,4/50) and an f-stop of f/16. The resulting spatial resolution in the PIV measurement plane is 56 μm.

4 Results

In this section, the measurement results are described, starting in Sect. 4.1 with the velocity field $\mathbf{v}(\mathbf{r})$ measured with PIV in the planes M1, M2, and M3. In Sect. 4.2, the experimental measurement of the mean position error $\overline{\xi}(\mathbf{r})$ is compared to the simulated position error $\overline{\xi}_{BOS}$. Furthermore, an estimation of systematic velocity errors $\Delta\mathbf{v}(\mathbf{r})$ of the PIV measurements is determined. In Sect. 4.3, random velocity errors $\sigma_{\Delta v}$ are estimated by error propagation of the measured position error ξ and the velocity field $\mathbf{v}$. As the velocity errors show only significant values in x-direction, the results are depicted only for the x-component.

4.1 PIV measurement results

Figure 5 shows the mean velocity field $\overline{\mathbf{v}}(\mathbf{r})$ and the corresponding standard deviation of the x-component of the velocity σ_{v_x} in the measurement planes M1, M2, and M3. The velocity field is measured by 500 single PIV measurements captured with 15 Hz repetition rate and a separation time of 400 μm. A commercial iterative PIV evaluation algorithm from Dantec Dynamics is used with a minimal

Fig. 5 Measured mean velocity field of 500 single measurements in the planes M1 (**a**), M2 (**b**) and M3 (**c**) and the corresponding standard deviation of the x-component of the velocity σ_{v_x} (**d**)–(**f**)
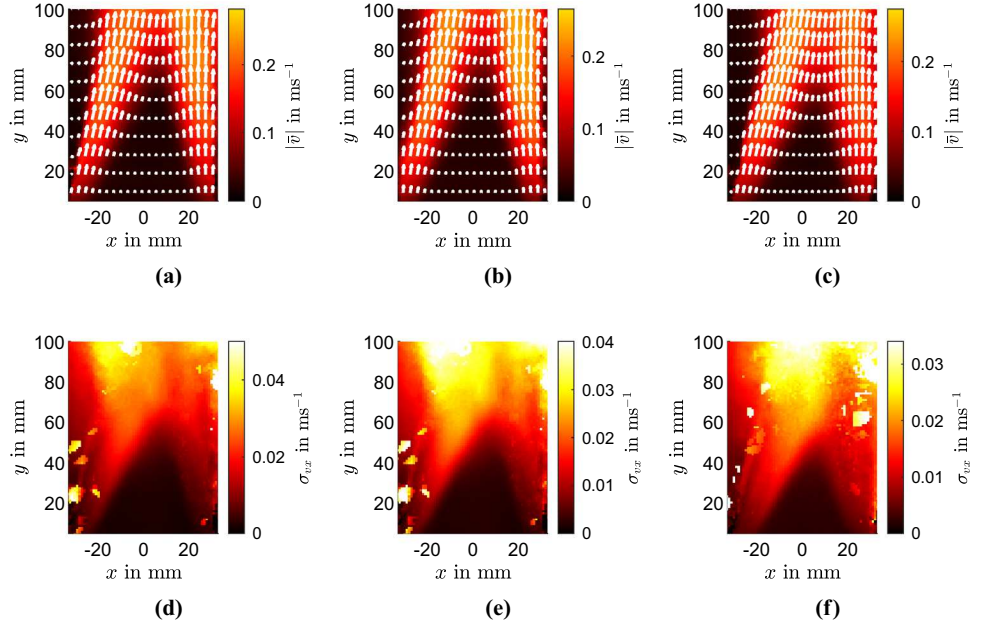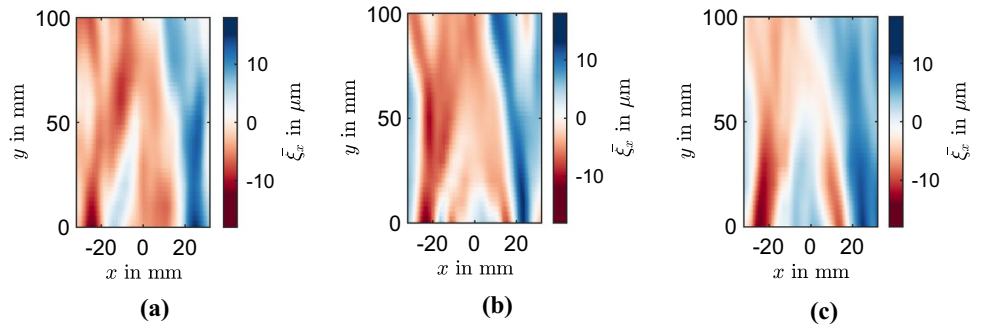
interrogation window size of $16 \times 16\,\mathrm{px}^2$ without overlap and with image deformation. The maximal velocity amounts up to $0.24\,\mathrm{m\,s^{-1}}$ and is located around the flame front, which exhibits a conical shape. The maximal standard deviation of the x-component of the velocity σ_{v_x} is located in the bright diffusive region of the flame, where the flame tends to fluctuate, and amounts up to about $0.05\,\mathrm{m\,s^{-1}}$, cf. Fig. 3b. The mean flow velocity shows a minor clockwise tilted direction, which leads to a slightly skewed symmetry axis.

4.2 Systematic velocity error

The relative systematic velocity error $\frac{\overline{\Delta v_i}}{\overline{v_i}}$ is determined by the insertion of the mean position error $\overline{\xi}_i$ and the mean velocity $\overline{v}_i$ in Eq. (1). Figure 6 illustrates the mean position errors $\overline{\xi}_x$ in x-direction of the glass tip position in the considered measurement planes M1, M2, and M3 averaged over 500 single measurements. A two dimensional Gaussian filter with a standard deviation of $1.6\,\mathrm{mm}$ is applied to reduce the noise. The resulting position error inside the flame can be qualitatively explained by the temperature distribution,

which is the dominating source of the refractive index field in premixed flames (Stella et al. 2001) and has its maximum in the flame front. The temperature distribution results in a density variation of the medium, which gives rise to a refractive index change. The connection between the density and the refractive index field is described by the Gladstone–Dale relation. Thus, high position errors occur in the region at $x \approx \pm 25\,\mathrm{mm}$ in Fig. 6, where high temperature gradients are located between the flame front and ambient air at room temperature. Inside the flame, the temperature gradients are inverted due to the internal premixed gas flow at about room temperature. Therefore, in the lower part of the flame at $y < 40\,\mathrm{mm}$, where the internal unburned premixed gas flow exists, there are local extrema at $x \approx \pm 18\,\mathrm{mm}$ in Fig. 6.

As the qualitative course of the particle position error can be explained by the temperature field, the quantitative results of the mean particle position error are validated by the comparison with ray-tracing simulations based on the mean refractive index field of the flame measured by BOS. The mean deflection angles ε of 100 single BOS measurements are derived from the position errors $\overline{\xi}_x$ of the recorded

Fig. 6 Measured particle position error $\overline{\xi}_x$ in the planes M1 (**a**), M2 (**b**), and M3 (**c**)

Fig. 7 Simulated particle position errors $\overline{\xi}_{\mathrm{BOS}}$ in the planes M1 (**a**), M2 (**b**), and M3 (**c**) based on the mean refractive index field measured by BOS
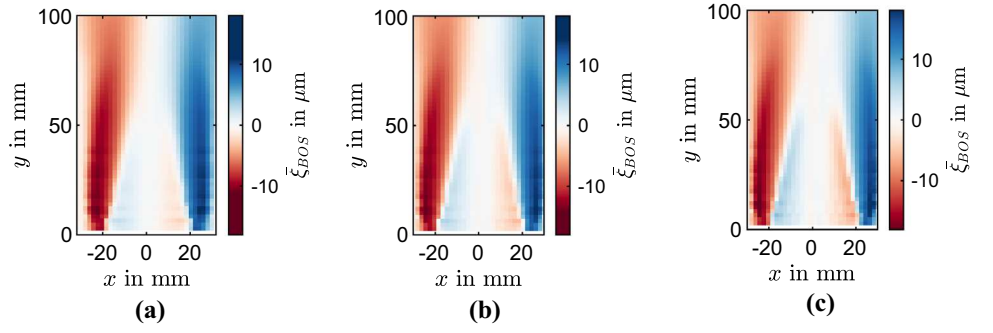
background pattern, which are calculated by a commercial adaptive PIV evaluation algorithm (Dantec Dynamics) with a final interrogation window size and grid size of $16 \times 16\,\mathrm{px}^2$. To confirm the measured particle position errors $\overline{\xi}_x$, the mean three-dimensional refractive index field $n(\mathbf{r})$ is reconstructed using the Abel–Fourier–Hankel method described in Sect. 2.2 with an ambient refractive index of $1 + 2.93 \times 10^{-4}$. The mean deflection angles ϵ were averaged over 100 single measurements. The fluctuations of the flame result in an average ratio of 1.5 between the standard deviation of the measured deflection angles and the mean deflection angles. In the Abel–Fourier–Hankel reconstruction of the mean refractive index field, the inclination of the flame is taken into account by adjusting the axis of symmetry, which is approximated by a second order polynomial. The polynomial line is fitted in the horizontal (y =const) arithmetic mean of the x-coordinates of the measured deflection angles ϵ weighted by the absolute deflection angle. A minimum refractive index of $n_{\min} = 1 + 0.41 \times 10^{-4}$ is calculated considering the smallest 0.5 % of the calculated refractive index as outliers. The minimum refractive index is used to estimate the maximum temperature in the flame using the Gladstone–Dale relation for a gas mixture of propane and air: (Merzkirch 2012)

$$n - 1 = K_{\mathrm{a}}\rho_{\mathrm{a}} + K_{\mathrm{p}}\rho_{\mathrm{p}}, \tag{5}$$

where $K_{\mathrm{a}} = 2.3 \times 10^{-4}\,\mathrm{m}^3\,\mathrm{kg}^{-1}$ and $K_{\mathrm{p}} = 2.3 \times 10^{-4}\,\mathrm{m}^3\,\mathrm{kg}^{-1}$ are the Gladstone–Dale constants of air and propane and ρ_{a} and ρ_{p} are the partial densities of air and propane, respectively. Here, it is assumed that the Gladstone–Dale constants of propane and air are also a valid description of the refractive index depending on the density for the reaction zone in the flame. This is justified due to the fact that the Gladstone–Dale constant does not depend on the chemical bonding in molecules (Stella et al. 2000). Furthermore, it is assumed that the volume fraction of $\frac{V_{\mathrm{a}}}{V_{\mathrm{p}}} = \frac{10}{1}$ remain constant in the reacting zone of the premixed flame. A maximum temperature of $T_{\max} = 1631\,°\mathrm{C}$ is estimated using

$$T = \frac{(n_0 - 1) \cdot T_0}{n - 1}, \tag{6}$$

where $n_0 = 1 + 2.7 \times 10^{-4}$ and $T_0 = 273.15\,\mathrm{K}$ are the reference refractive index and the reference temperature at room temperature, respectively. The estimated maximal temperature is sufficiently lower than the softening temperature of the quartz glass of $1730\,°\mathrm{C}$.

Based on the reconstructed mean refractive index field, ray-tracing simulations of the particle position error $\overline{\xi}_{\mathrm{BOS}}$ are performed in the measurement planes M1, M2, and M3 shown in Fig. 7. Compared to the mean measured particle position errors $\overline{\xi}_x$ in Fig. 6, the simulated particle position errors $\overline{\xi}_{\mathrm{BOS}}$ show qualitative accordance. Although, the results from the simulations appear smoother than the measured position errors, which results from the spatial smoothing characteristics of the BOS measurement and the Abel–Fourier–Hankel method. For a quantitative comparison, the measured position error $\overline{\xi}_x$ and the simulated position error $\overline{\xi}_{\mathrm{BOS}}$ are plotted for $y = 10\,\mathrm{mm}$ and $z = 0\,\mathrm{mm}$ in Fig. 8a. In addition, the radial temperature gradients in the same measurement plane are calculated using Eq. (6) and depicted in Fig. 8b. The error bars in Fig. 8a represent the standard deviation of the single measurement values with a coverage factor of $k = 1$. In the region from $x \approx -5\,\mathrm{mm}$ to $x \approx 15\,\mathrm{mm}$, the measured position errors show an asymmetric course, which is not mapped by the simulated position errors. This discrepancy can be explained by the implicit assumption of an axisymmetric refractive index field for the Abel–Fourier–Hankel method. Furthermore, the asymmetric condition results in a non-zero position error measured at $x = 0\,\mathrm{mm}$. For an axisymmetric flame, the gradients of the refractive index should be aligned perpendicular to the observation direction. In the examined flame, this perpendicular condition seems to be fulfilled at $x \approx -8\,\mathrm{mm}$ due to a deformed flame front, which is not apparent in the simulated position error due to the implicit assumption of an axisymmetric refractive index field. Apart from the region from $x = -5\,\mathrm{mm}$ to $x \approx 15\,\mathrm{mm}$, the results indicate quantitative agreement within the scope of the depicted error bars. Particularly, in the region around the flame front with the highest position errors at $x \approx \pm 25\,\mathrm{mm}$, the simulated and measured position error shows only small deviations. Here, also the highest velocity errors occur.
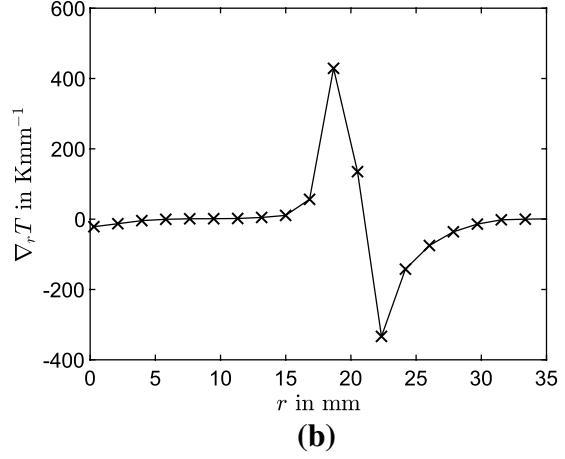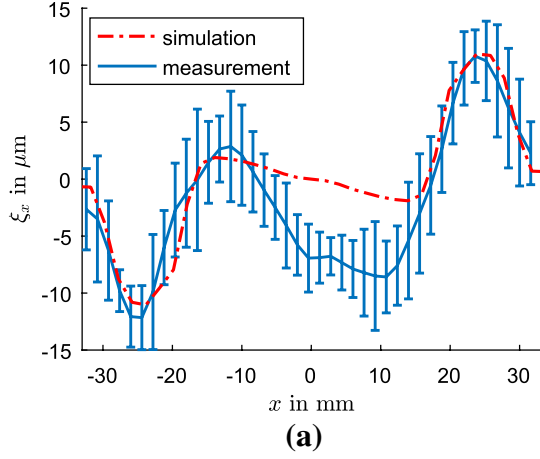
Fig. 8 Quantitative comparison between the simulated and the measured position error at $y = 10\,\text{mm}$. **a** Comparison between the Gaussian filtered direct measurement of the position error $\overline{\xi}_x$ and the simulated position error $\overline{\xi}_{\text{BOS}}$. **b** Calculated axial symmetric temperature gradient $\nabla_r T$ for the radius r based on the mean refractive index field measured with BOS

Fig. 9 Relative systematic measurement error $\left|\frac{\overline{\Delta v_x}}{\tilde{v}_x}\right|$ of the PIV measurement caused by particle position error in the planes M1 (**a**), M2 (**b**), and M3 (**c**)
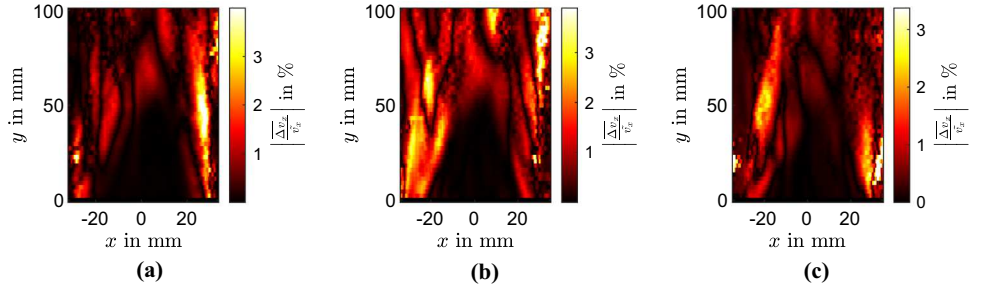
The particle position errors $\overline{\xi}_x(\mathbf{r})$ and the velocity fields $\mathbf{v}(\mathbf{r})$ in the planes M1, M2, and M3 inside the combustion flow were measured with a glass rod and with PIV, respectively. With Eq. (1), an estimation of the systematic velocity error inside the flame flow is performed and the resulting systematic measurement error of the mean velocity field standardized to the mean velocity of the entire flow $\tilde{v}_x$ is depicted in Fig. 9. The highest 0.5 % of the resulting systematic velocity error values are truncated to ignore outliers. The maxima are located around the flame front, where the velocity gradients $\nabla_x \overline{v}_x$, the particle position error $\overline{\xi}_x$, and its gradient $\nabla_x \overline{\xi}_x$ show high values. The reduction of the maximal systematic error regarding the measurement planes M2 and M3 seems to be counterintuitive, because the propagation distance of the reflected light inside the refractive index field increases. Though, the reduction of the systematic error can be explained by the light paths inside the refractive index field. The reflected light of the particles or rather the glass rod tip is spatially filtered by the spatial angle of the aperture of the camera objective. Therefore, diverging light rays from the object are detected, and consequently, the light rays are affected by different refractive index values resulting in a spatial filter of the affecting refractive index field. The spatial filter smooths the refractive index edge at the border of the flame front and reduces the occurring systematic velocity error. However, it can also be assumed that the particle images appear blurred, and thus, the signal-to-noise ratio will be reduced. Anyway, systematic velocity errors of at least 3% to 4% occur in the examined measurement planes inside the flame. Hence, compared to the typical PIV measurement uncertainty of about 1% to 2% (Westerweel 1997; Voges et al. 2007), the effect of light refraction inside flame flows due to refractive index fields can lead to significant systematic measurement errors in the region around the flame front. This region is also of particular interest for studying the dynamics of combustion chemistry (Kiefer et al. 2008; Schlüßler et al. 2015), which requires high precision and reliable velocity data. To achieve that, the accuracy of the velocity data can be improved by the correction of the quantified velocity error depicted in Fig. 9.

Fig. 10 Relative random measurement error $\frac{\sigma_{\Delta v_x}}{\tilde{v}_x}$ of the PIV measurement caused by particle position error in the planes M1 (**a**), M2 (**b**), and M3 (**c**)
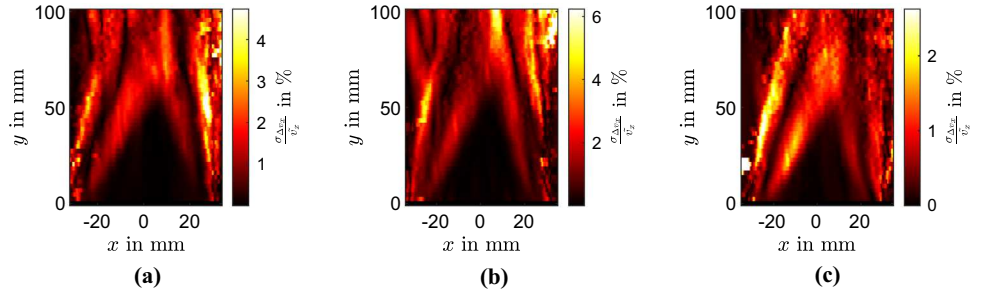
4.3 Random velocity error

In Fig. 10, the resulting random measurement error is depicted, which is calculated with Eq. (2) and standardized to the mean velocity of the entire flow $\tilde{v}_x$ in x-direction. Again, the highest 0.5% of the resulting systematic velocity error values are truncated to ignore outliers. Like the maximal systematic errors, also the maximal random velocity errors are located in the region around the flame front. However, compared to the systematic measurement errors, the random measurement errors vary more intense in the examined measurement planes with a maximum of about 6% , which will lead to an increased measurement uncertainty for the turbulence statistics of the flame.

5 Conclusion

The measurement error of the particle position in PIV measurements due to inhomogeneous refractive index fields inside combustion flows leads to velocity measurement errors. To get quantitative information about resulting PIV measurement errors, a direct measurement approach is proposed for the determination of occurring particle position errors inside combustion flows. The experimental approach is based on the position measurement of a glass rod tip inserted into the flame. The results of the measured systematic position error are verified by the comparison to ray-tracing simulations based on the mean refractive index field measured with BOS.

As an example, the proposed measurement approach is applied to a premixed propane flame. Since the measurement error of the particle position depends on the distance of the scattering light path between the particles and the camera, the position error was determined in three different measurement planes located at the center of the flame flow and 3 mm and 6 mm behind the center of the flow with respect to the viewing direction of the camera. The resulting maximal relative systematic measurement errors were found to be 3% to 4% for the examined measurement planes. A significant increase of the systematic measurement errors with respect to a 6 mm increased optical path length inside the refractive

index field of the flame was not observed. The random measurement errors were estimated by means of error propagation of the measured position error and the measured velocity, which results in a maximal relative random velocity error between 4% and 6%. Moreover, the random error appears to be more sensitive with respect to the optical paths within the inhomogeneous refractive index field. The significant random velocity error will result in an increased measurement uncertainty of the turbulence statistics.

Note that, the resulting measurement errors are sensitive to the dimension of the examined flame or rather the inhomogeneous refractive index field. Besides the optical path length inside the refractive index field, also the maximal temperatures, the mixing ratio between the fuel and oxidant as well as the used fuel influence the refractive index. Thus, all these parameters affect the resulting measurement errors. The estimated PIV measurement errors, therefore, have to be considered individually for various measurement setups and cannot be extrapolated to other configurations. In conclusion, the systematic as well as the random measurement errors can significantly affect the PIV measurement inside flame flows, where the largest measurement errors occur in the region of the flame front. Therefore, for precise measurements inside larger flame flows, the measurement uncertainty due to light refraction is problematic and should be taken into account. This is particularly important when the experimental data are used to validate results from numerical simulations (Barlow 2007), e.g., by Reynolds-averaged Navier Stokes (RANS) or large eddy simulations (LES).

In addition, besides the PIV measurement error induced by light refraction, also the thermophoresis leads to measurement errors inside flame flows. Since the light refraction and the thermophoresis mainly affect the PIV measurement accuracy in the region of the flame front, a compensation or an increase of the individual measurement errors can result. Furthermore, the resulting measurement errors of stereoscopic and tomographic PIV due to inhomogenous refractive index fields inside combustion flows remain unknown. For an estimation of these errors, multiple camera perspectives have to be considered. Here, even higher velocity errors can be expected as the results from Vanselow and Fischer (2018) for the investigation of resulting PIV measurement errors

inside an inhomogeneous refractive index field of a hot jet flow show.

References

Barlow RS (2007) Laser diagnostics and their interplay with computations to understand turbulent combustion. Proc Combust Inst 31(1):49–75

Elsinga GE, van Oudheusden BW, Scarano F (2005) Evaluation of aero-optical distortion effects in PIV. Exp Fluids 39(2):246–256

Fischer A (2016) Fundamental uncertainty limit of optical flow velocimetry according to Heisenberg's uncertainty principle. Appl Opt 55(31):8787

Fischer A (2017) Imaging flow velocimetry with laser mie scattering. Appl Sci 7(12):1298

Fischer A, König J, Czarske J, Peterleithner J, Woisetschläger J, Leitgeb T (2013) Analysis of flow and density oscillations in a swirl-stabilized flame employing highly resolving optical measurement techniques. Exp Fluids 54(12):1622

Kiefer J, Li ZS, Zetterberg J, Bai XS, Aldén M (2008) Investigation of local flame structures and statistics in partially premixed turbulent jet flames using simultaneous single-shot CH and OH planar laser-induced fluorescence imaging. Combust Flame 154(4):802–818

Merzkirch W (2012) Flow visualization. Academic Press, Cambridge

Nobach H, Bodenschatz E (2009) Limitations of accuracy in PIV due to individual variations of particle image intensities. Exp Fluids 47(1):27–38

Nogenmyr KJ, Kiefer J, Li ZS, Bai XS, Aldén M (2010) Numerical computations and optical diagnostics of unsteady partially premixed methane/air flames. Combust Flame 157(5):915–924

Raffel M (2015) Background-oriented schlieren (BOS) techniques. Exp Fluids 56(3):60

Raffel M, Willert C, Kompenhans J (2002) Particle image velocimetry: a practical guide (experimental fluid mechanics). Springer, Berlin

Schlüßler R, Czarske J, Fischer A (2014) Uncertainty of flow velocity measurements due to refractive index fluctuations. Opt Lasers Eng 54:93–104

Schlüßler R, Bermuske M, Czarske J, Fischer A (2015) Simultaneous three-component velocity measurements in a swirl-stabilized flame. Exp Fluids 56(10):183

Sharma A, Kumar DV, Ghatak AK (1982) Tracing rays through graded-index media: a new method. Appl Opt 21(6):984

Steinberg AM, Boxx I, Stöhr M, Carter CD, Meier W (2010) Flow flame interactions causing acoustically coupled heat release fluctuations in a thermo-acoustically unstable gas turbine model combustor. Combust Flame 157(12):2250–2266

Stella A, Guj G, Giammartini S (2000) Measurement of axisymmetric temperature fields using reference beam and shearing interferometry for application to flames. Exp Fluids 29(1):1–12. https://doi.org/10.1007/s003480050420

Stella A, Guj G, Kompenhans J, Raffel M, Richard H (2001) Application of particle image velocimetry to combusting flows: design considerations and uncertainty assessment. Exp Fluids 30(2):167–180

Tan DJ, Edgington-Mitchell D, Honnery D (2015) Measurement of density in axisymmetric jets using a novel background-oriented schlieren (BOS) technique. Exp Fluids 56(11):204

Vanselow C, Fischer A (2018) Influence of inhomogeneous refractive index fields on particle image velocimetry. Opt Lasers Eng 107:221–230

Voges M, Beversdorff M, Willert C, Krain H (2007) Application of particle image velocimetry to a transonic centrifugal compressor. Exp Fluids 43(2):371–384

Westerweel J (1997) Fundamentals of digital particle image velocimetry. Meas Sci Technol 8(12):1379